

Physics at International Linear Collider (ILC)

Hitoshi YAMAMOTO*

Graduate School of Science, Tohoku University, Sendai 980-8578

(Received June 20, 2007; accepted August 27, 2007; published November 12, 2007)

International Linear Collider (ILC) is an electron–positron collider with the initial center-of-mass energy of 500 GeV which is upgradable to about 1 TeV later on. Its goal is to study the physics at TeV scale with unprecedented high sensitivities. The main topics include precision measurements of the Higgs particle properties, studies of supersymmetric particles and the underlying theoretical structure if supersymmetry turns out to be realized in nature, probing alternative possibilities for the origin of mass, and the cosmological connections thereof. In many channels, Higgs and leptonic sector in particular, ILC is substantially more sensitive than LHC, and is complementary to LHC overall. In this short article, we will have a quick look at the capabilities of ILC.

KEYWORDS: ILC, Higgs boson, New Physics, supersymmetry, extra dimensions, cosmology, LHC
DOI: [10.1143/JPSJ.76.111014](https://doi.org/10.1143/JPSJ.76.111014)

1. Introduction

The standard model is an astonishingly successful theory in describing what have been observed in the field of elementary particles. The Higgs particle, which gives mass to all massive particles, is at the core of the standard model, but so far has not been found. Furthermore, if one tries to calculate the radiative correction to the mass squared of Higgs, it diverges quadratically with the cut off energy, and if one assumes that the standard model is correct up to the energy scale of the grand unification ($\sim 10^{16}$ GeV), the correction to the Higgs mass becomes the order of the grand unification scale itself. Since precision measurements so far shows that the standard model Higgs should lie below ~ 200 GeV, this is only possible if the original mass and the correction are canceling out to an astonishing precision. This unpleasant situation is referred to as the fine-tuning problem, or the naturalness problem. The problem is in part caused by the large difference in energy scale from the Higgs mass to the grand unification scale, and in this context, it is referred to as the hierarchy problem.¹⁾ Also, the standard model does not include the gravitational force.

A theoretical solution to the fine-tuning problem is provided by supersymmetry (SUSY)²⁾ which postulates that every particle in the standard model has its so-called super-partner (called a super particle or a s-particle) whose spin differs by one half from that of the original particle. Not only the inclusion of the super particles naturally cancels out the quadratic divergence of the Higgs mass correction, in SUSY the gauge coupling constants converges to a single value at the grand unification scale. Furthermore, the gravitational force can also be naturally incorporated in SUSY. As a bonus, SUSY has candidates for the dark matter which is thought to consist of unknown stable massive particles and accounts for one quarter of the energy of the universe.

Even though SUSY is an attractive theory with many merits for us, nature of course would not care about our conveniences. There are several alternative models that address the fine-tuning problem, and some of them may have

connection to the reality of nature. Examples are the models with extra dimensions which postulate the existence of space dimensions more than our 3 (space) + 1 (time) dimensions,³⁾ and the little Higgs model⁴⁾ where the Higgs particle is considered to be composite.

The physics potential of ILC has been extensively studied and documented.^{5–9)} As we will see below, the standard model Higgs particle will have distinctive signals at ILC, and SUSY and other alternative models also have many possibilities of being found and studied at ILC. The advantage of ILC with respect to LHC is in the general cleanliness of the events where two elementary particles (an electron and a positron) with known kinematics and spin define the initial state, and the high resolutions of the detector that are made possible by the relatively low absolute rate of background events. The capability of ILC is further enhanced by the options such as the $\gamma\gamma$ collision, e^-e^- collision, and Z-pole running (“Giga-Z”).

2. ILC Machine Parameters and Detectors

The basic parameters, such as energy and luminosity, of ILC are described in the parameter report.¹⁰⁾ The baseline machine allows for a center-of-mass energy range between 200 and 500 GeV and luminosity of 500 fb^{-1} in the first four years of running not counting the year zero. The energy scan is possible at any energy within the range, and the electron polarization is at least 80%. Two detectors are expected which may be in a push–pull configuration.

For each of the two beams, a bunch is $\sigma_y = 5.7$ nm high, $\sigma_x = 655$ nm wide, and $\sigma_z = 300 \mu\text{m}$ long, and contains 2×10^{10} particles. About 3000 bunches with 308 ns bunch separation form a train of about 1 ms which comes with 5 Hz repetition rate. The collision occurs with crossing angle of 14 mrad.

The highest priority beyond the baseline is the energy upgrade to approximately 1 TeV, and the upgraded machine should be able to collect 1 ab^{-1} in 3 to 4 years after the baseline running. The options include: running at 500 GeV to double the luminosity to 1 ab^{-1} , e^-e^- collision, positron polarization of 50% or more, Z-pole running, WW threshold running, and $\gamma\gamma$ and $e^- \gamma$ collisions using backscattered laser

*E-mail: yhitoshi@awa.tohoku.ac.jp

beams. The priorities of these options will depend on the results of LHC and the baseline ILC.¹¹⁾ In the following, the baseline machine with 200 to 500 GeV center-of-mass energy is assumed unless stated otherwise.

The physics of ILC is realized through synthesis of unprecedented performances of both machine and detectors. ILC detectors can take advantage of the relatively low rates and low radiation doses to achieve momentum resolution that is order of magnitude better, jet energy resolution factor of two better, and the vertex resolution several times better than those at the previous electron–positron colliders. As we will see below, these performances are not overkill; rather, they are needed to realize the physics potential of ILC.

3. Standard Model Particles

We start from the particles that are ingredients of the standard model. Their properties and interactions with other particles, however, may reveal physics beyond the standard model. The goal is to look at the behavior of the members of the standard model to see if there is any hint of new physics. Production cross sections for some standard model particles as well as those for particles beyond the standard model are shown in Fig. 1.

3.1 Gauge bosons

Non-Abelian nature of gauge group leads to couplings among gauge bosons, and their pattern reflects the structure of the underlying gauge group. W -pair creation $e^+e^- \rightarrow W^+W^-$ is highly sensitive to the triple gauge couplings $WW\gamma$ and WWZ which can be separated by beam polarizations. With 90 and 60% for electron and positron

polarizations, respectively, and 500 fb^{-1} at $\sqrt{s} = 500 \text{ GeV}$ and 1 ab^{-1} at $\sqrt{s} = 800 \text{ GeV}$, anomalous couplings can be measured with typical errors of 10^{-3} relative.¹²⁾ The $WW\gamma$ magnetic dipole coupling κ_γ , in particular, can be measured to 10^{-4} , which is more than order of magnitude better than LHC with the same years of running. The triple gauge coupling $WW\gamma$ can also be studied by the single gauge boson productions $e^+e^- \rightarrow e^- \nu W^+$, $\nu \nu Z$, and also by the $e\gamma$ and $\gamma\gamma$ options; namely, $e^- \gamma \rightarrow W^- \gamma$ and $\gamma\gamma \rightarrow W^+W^-$ where the WWZ coupling does not contribute.

If Higgs is not found at LHC or ILC, it may indicate that W -pair can form a bound state which could be found in the WW scattering process $e^-e^+ \rightarrow \nu\bar{\nu}W^+W^-$ as a resonance or anomalous quartic gauge couplings. Quartic gauge couplings can generally be probed by gauge boson scattering processes of the type $e^-e^+ \rightarrow VVff$ where V is W or Z and f is e or ν , or by triple gauge boson productions $e^-e^+ \rightarrow VVV$. At ILC, one can tell the initial and final states of the gauge boson scatterings, which is often difficult at LHC.

If no Higgs or no new particles are found, precision measurements on Z become important. The Giga- Z option can collect 1 billion Z 's in a few months, and can improve by more than one order of magnitude those measurements that use b -tagging and/or beam polarizations.¹³⁾ The improved b -tagging is realized by the excellent vertexing capability of ILC detectors.

Couplings of fermions and gauge boson can also be studied by $e^+e^- \rightarrow f\bar{f}$ (f stands for a fermion), where anomalous couplings may be parametrized by $(1/\Lambda_{ij}^2)(\bar{e}_i\gamma^\mu e_i)(\bar{f}_j\gamma_\mu f_j)$ ($ij = L, R$). ILC is sensitive to Λ_{ij} of typically 20 to 100 TeV.¹⁴⁾

The $e^+e^- \rightarrow f\bar{f}$ modes are also sensitive to existence of an extra Z boson (Z') even when the mass of Z' is above the CM energy. Such extra gauge bosons appear in many extensions of the standard model. Some examples are the E_6 χ model (χ), left–right symmetric model (LR), Littlest Higgs model (LH), Simplest Little Higgs model (SLH), and model with extra dimensions where Z' particles are actually spin-2 Kaluza–Klein excitations of gravitons (KK). The signatures appear in the forward-backward asymmetry of the $f\bar{f}$ production and in the dependence of the cross section on the beam polarization. The resolving power of ILC in the two-dimensional space of C_L^ℓ and C_R^ℓ is shown in Fig. 2 for $e^+e^- \rightarrow \mu^+\mu^-$, where $C_{L,R}^\ell$ are the left- and right-handed $Z'\ell$ coupling coefficients where the lepton universality is assumed. Electron and positron polarizations of 80 and 60% respectively, are assumed. There are quadratic ambiguities due to the sign-independence of coupling coefficients. LHC may find a Z' resonance, but it would take ILC to identify the underlying theory.

3.2 Top quark

The top quark is the heaviest elementary particle observed so far, and its mass $\sim 174 \text{ GeV}$ is in the range of the electroweak symmetry breaking. Its large mass indicates that it couples to Higgs strongly and thus should be sensitive to the structures in the Higgs sector, or whatever is responsible for creation of masses. In many models beyond the standard model, the Higgs mass strongly depends on the top mass. In MSSM (the minimal supersymmetric standard model), for example, an error in the top mass corresponds to a similar

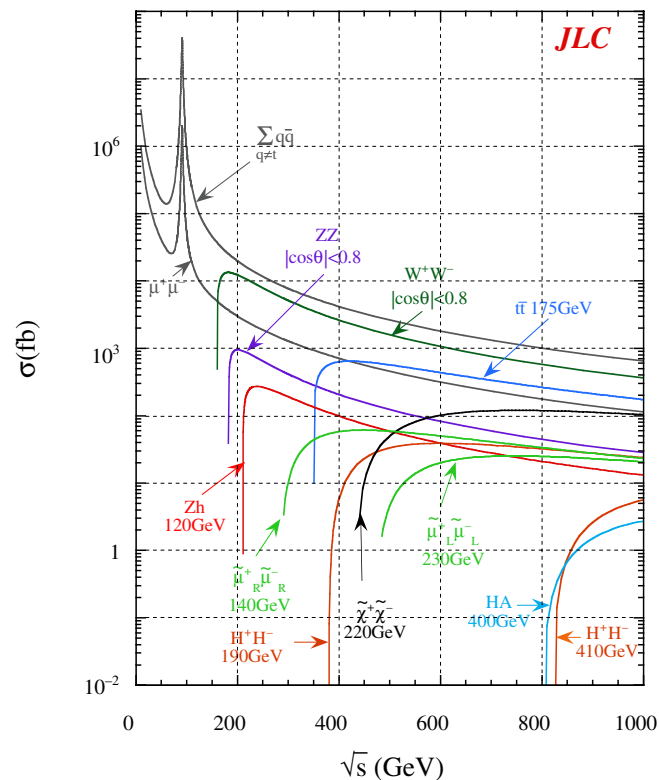


Fig. 1. (Color online) Production cross sections for some standard model particles as well as for new physics particles at e^+e^- collider as functions of CM energy.⁶⁾

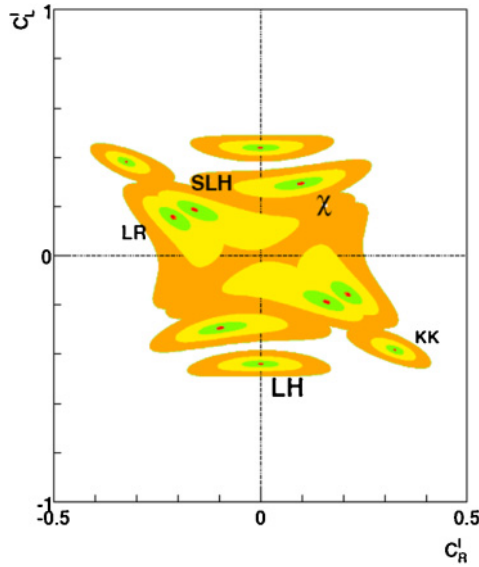


Fig. 2. (Color online) The 95% confidence level regions for various models using $e^+e^- \rightarrow$ lepton pair.¹⁶⁾ The regions correspond to $m_{Z'}$ = 1, 2, 3, 4 TeV with the smallest region is for 1 TeV.

error in the Higgs mass, which means that precision measurements of the top and Higgs masses serve as a stringent test of theoretical models. In some cases, non-standard top couplings may be the only area new physics can be found.

The top mass m_t is best measured by the $e^+e^- \rightarrow t\bar{t}$ threshold scan, taking about 5 fb^{-1} each at several points of CM energy. Since the top quark decays before it hadronizes, the excitation curve, i.e., the cross section as a function of CM energy, around the threshold can reliably be calculated. It is affected by the beam energy spread, initial-state radiation, beamstrahlung (radiation from a beam particle under the coherent electromagnetic field of the incoming bunch), as well as the higher order corrections which has been performed up to including some of the next-to-next-to-leading logarithms (NNLL).¹⁵⁾ The experimental and theoretical uncertainties are of the same order, and the resulting overall error on m_t is expected to be 100 to 200 MeV which can be compared to 1 to 2 GeV at LHC. The threshold scan also yield the top width to a few percent of its value which is around 1.5 GeV.

The production and decay of top quark in $e^+e^- \rightarrow t\bar{t}$, $t \rightarrow bW$ can be studied near the threshold, well above the threshold, or below the threshold (where one of the top quark is off-shell). The production is sensitive to ttZ and $tt\gamma$ couplings and the decay is sensitive to tbW coupling. Many beyond-the-standard models predict deviations in these couplings from the standard-model values. The models with fourth generation with large mixing between fourth and third generations of quarks would have the tbW coupling smaller than that of the standard model while the ttZ coupling would be the same. The little Higgs models with T-parity and the top flavor models would have both tbW and ttZ couplings smaller than those of the standard model. Figure 3 shows the sensitivities of ILC and LHC on the axial ttZ coupling and the left-handed tbW coupling as well as the expected deviations for the top-flavor model and the little-Higgs model with T-parity, and the model with fourth generation.

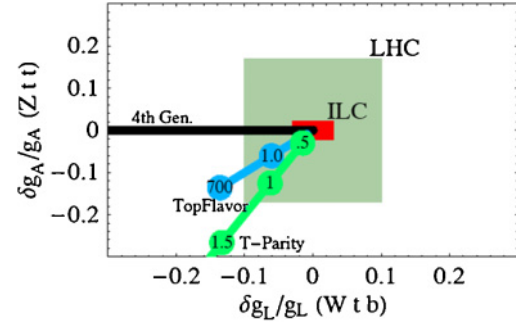


Fig. 3. (Color online) Sensitivities of ILC and LHC on the axial ttZ coupling and the left-handed tbW coupling.¹⁷⁾ The expected deviations for the top-flavor model and the little-Higgs model with T-parity, and the model with fourth generation are also shown.

of the Higgs-top- (top partner) coupling and those on the line for the top flavor model are the mass of the extra Z boson. Furthermore, the KK mode of graviton with mass 10 to 100 TeV in Randall–Sundrum models¹⁸⁾ may be indirectly detected as anomalous $t\bar{t}$ production.

3.3 Higgs particle

Our current knowledge on the mass of the Higgs particle mainly comes from the LEP experiments.¹⁹⁾ Within the framework of the standard model, Higgs mass m_H is bounded as $114.4 < m_H < 166 \text{ GeV}$ at 95% confidence level, where the lower limit is from direct searches and the upper limit is by an overall fit of the standard model parameters to the data. On the other hand, Higgs in the MSSM is constrained to be less than 135 GeV, which is lower than the upper limit in the standard model. These Higgs particle, if they exist, will be found at LHC within the first few years of running. At ILC, even though the start would be many years later than LHC, the same level of discovery sensitivity can be obtained by one day of running at the design luminosity. With its clean initial and final states, and high resolutions of the ILC detectors, ILC will be able to perform measurements on spin and parity of the Higgs particle, and determine coupling strengths to various particles model-independent ways.

The primary production channels of the standard model Higgs are $e^+e^- \rightarrow Z^* \rightarrow ZH$ (Higgs-strahlung) and $e^+e^- \rightarrow \nu\bar{\nu}H$ (WW fusion) as shown in Fig. 4. The Higgs-strahlung dominates at low CM energies ($< 500 \text{ GeV}$) and the WW fusion dominates at high CM energies ($\sim 1 \text{ TeV}$). For m_H of 120 GeV, an integrated luminosity of 500 fb^{-1} at CM energy of 500 GeV will generate $(3-4) \times 10^4$ Higgs particles in each of the two production channels. The decay branching fractions of Higgs are shown in Fig. 5. If the

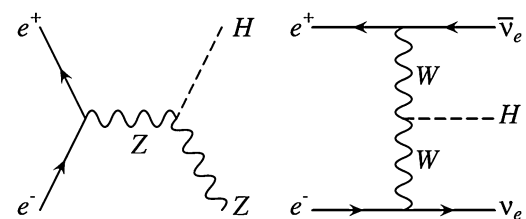


Fig. 4. The main Higgs production mechanisms at ILC: the Higgs-strahlung (left) and the WW fusion (right).

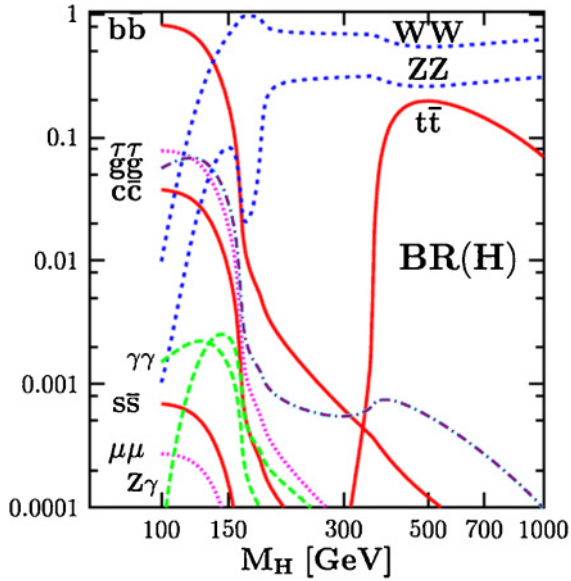


Fig. 5. (Color online) Higgs decay branching fractions as functions of Higgs mass.²¹⁾

Higgs mass is below around 140 GeV, it decays primarily to $b\bar{b}$ with a few % each for $c\bar{c}$, $\tau\bar{\tau}$, and gg branching fractions. The width of Higgs in this mass range is less than 10 MeV. For m_H larger than around 150 GeV, it decays primarily to WW with the ZZ channel following at 20% level. The $t\bar{t}$ final state opens for m_H larger than around 350 GeV and peaks for $m_H \sim 500$ GeV at 20% branching fraction. At m_H of around 500 GeV, the Higgs is quite broad with $\Gamma_H \sim 100$ GeV.

Figure 6 shows the recoil mass distribution for $e^+e^- \rightarrow ZH, Z \rightarrow \mu\mu$ with 500 fb^{-1} at CM energy of 300 GeV. Peaks corresponding to different values of m_H are shown together with the background from $e^+e^- \rightarrow ZZ$ followed by one or both of the Z 's decaying to $\mu\mu$. Since the Higgs particle is not reconstructed, the method is independent of the Higgs decay modes including the case where the decay is invisible. The range of detectable Higgs mass reaches close to the CM energy itself; more precisely, up to CM energy minus m_Z .

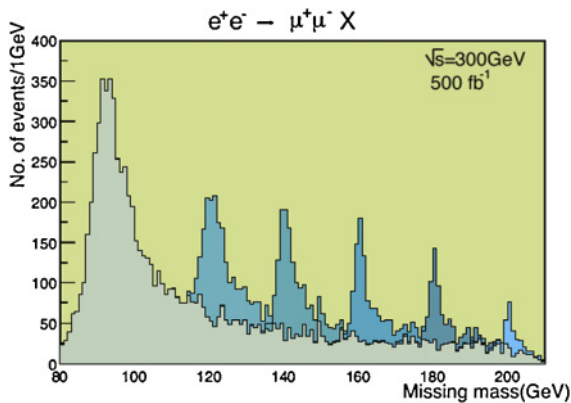


Fig. 6. (Color online) The $\mu\mu$ recoil mass distribution in $e^+e^- \rightarrow \mu\mu X$ with 500 fb^{-1} at CM energy of 300 GeV.⁶⁾ The peaks correspond to $e^+e^- \rightarrow ZH$ followed by $Z \rightarrow \mu\mu$ with different values of m_H , together with the background from $e^+e^- \rightarrow ZZ, Z \rightarrow \mu\mu$.⁷⁾

The Higgs mass is obtained from the recoil mass distribution itself. Under the same conditions used for Fig. 6, the error in m_H is ~ 70 MeV which improves to ~ 40 MeV if hadronic decays of Z are included. The spin and parity of the Higgs particle can be determined by the threshold excitation curve and the angular distribution of the Higgs production in the Higgs-strahlung process. If the rise of the cross section just above the threshold is $\sigma \propto \beta_H$, the ZH pair is in a S-wave. Then the parity conservation in $Z^* \rightarrow ZH$ indicates that the parity of Higgs is plus. At well above threshold, Z in the final state is mostly helicity 0. Since the intermediate Z^* is polarized along the beam direction, the angular distribution of spin-0 Higgs is given by $|d_{1,0}^1(\theta)|^2 \propto \sin^2 \theta$. The spin parity of Higgs can also be checked in $e^+e^- \rightarrow ZH \rightarrow f\bar{f}f\bar{f}$ or in $H \rightarrow WW^*, ZZ^* \rightarrow f\bar{f}f\bar{f}$ where f stands for a fermion.²²⁾ One can also study the spin correlation of the final state τ 's in $H \rightarrow \tau^+\tau^-$ to extract the CP of Higgs.²³⁾

The Higgs-strahlung process allows one to measure the ZZH coupling independently of the Higgs decay modes. On the other hand, the WW fusion process gives the WWH coupling. At low CM energy, the WW fusion process $e^+e^- \rightarrow \nu\bar{\nu}H$ has a substantial background coming from $e^+e^- \rightarrow ZH, Z \rightarrow \nu\bar{\nu}$ which can be removed by looking at the recoil mass of Higgs. Also, the WW fusion process can be turned off and on by switching the beam polarizations to identify the contribution from the WW fusion process. The WWH coupling can also be extracted from the $H \rightarrow WW^*$ branching fraction. The statistical errors on WWH and ZZH couplings for m_H of 120 GeV are 1–2%. For the Higgs mass below 150 GeV, the couplings of Higgs to b, c , and τ are measured by reconstructing the Higgs decays to $b\bar{b}, c\bar{c}$, and $\tau^+\tau^-$ in the Higgs-strahlung process. Here, the branching ratios are proportional to the square of the fermion mass, and the excellent vertexing capability of ILC detectors is essential in separating $c\bar{c}$ from $b\bar{b}$. The $t\bar{t}H$ Yukawa coupling is measured by $e^+e^- \rightarrow t\bar{t}^* \rightarrow t\bar{t}H$ at 1 TeV. The process $e^+e^- \rightarrow t\bar{t}$ is itself sensitive to the $t\bar{t}H$ coupling through the H -loop vertex correction. The gluonic decay $H \rightarrow gg$ as well as the decays $H \rightarrow \gamma\gamma, \gamma Z$ are sensitive to the $t\bar{t}H$ coupling though top loop, and also sensitive to new heavy particles that may contribute in the loop. For high Higgs masses, the gauge boson pair final states dominate. Still, with 1 ab^{-1} at 1 TeV, the $b\bar{b}$ branching fraction can be measured to 12 and 28% for $m_H = 180$ and 220 GeV, respectively. Invisible final state can also be found by the recoil mass technique, with 5σ confidence down to 2% branching fraction for $120 < m_H < 160$ GeV.

The total Higgs width for m_H less than ~ 200 GeV is too narrow to be measured directly, but can be indirectly measured by $\Gamma_H = \Gamma(H \rightarrow WW^*)/Br(H \rightarrow WW^*)$ where $Br(H \rightarrow WW^*)$ is directly measured and $\Gamma(H \rightarrow WW^*)$ is estimated from the measurement of the WWH coupling by, say, the WW fusion process. For $120 < m_H < 160$ GeV, the total Higgs width can be measured with an error of 4 to 13%.

The trilinear Higgs coupling, or the Higgs self coupling, can be measured by $e^+e^- \rightarrow ZH^* \rightarrow ZHH$ or by $e^+e^- \rightarrow \nu\bar{\nu}H^* \rightarrow \nu\bar{\nu}HH$. The cross section is quite small and the final state $(b\bar{b})(b\bar{b})(\ell^+\ell^-)$ challenges the capability of detector. Here, a superb vertexing resolution is critical for the b

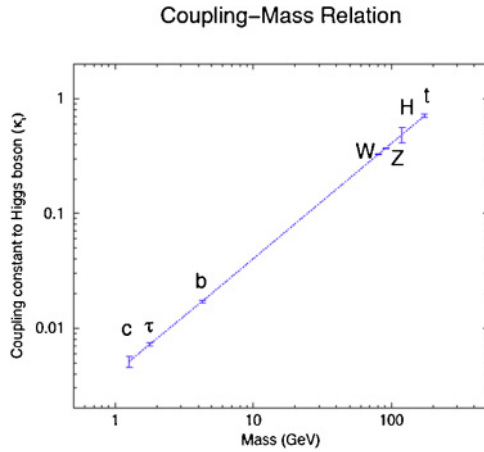


Fig. 7. (Color online) The Higgs coupling constants as functions of mass of the particle that Higgs couples to.⁷⁾ The couplings with gauge bosons and the self coupling are normalized differently from those with fermions.

tagging, and an excellent jet energy reconstruction is needed for calculating the invariant masses of b jet pairs. With 1 ab^{-1} at 500 GeV CM energy and for $m_H = 200 \text{ GeV}$, the error on the Higgs self coupling constant λ_{HHH} is estimated to be about 20% using the $e^+e^- \rightarrow ZH^* \rightarrow ZHH$ mode only.²⁴⁾ If one combines $e^+e^- \rightarrow ZHH$ and $e^+e^- \rightarrow \nu\bar{\nu}HH$ at 1 TeV CM energy, the error in λ_{HHH} becomes 12% for the same Higgs mass with 1 ab^{-1} and 80% electron polarization.²⁵⁾

Expected results for Higgs coupling measurements are plotted in Fig. 7 as functions of mass of the particle that Higgs couples to. Coupling constants of Higgs to fermions, weak bosons W and Z , and Higgs itself are given by m_f/a , gm_W , $gm_Z/2 \cos\theta_w$, and $m_H^2/2a$, respectively, where $g \sim 0.65$ is the $SU(2)$ coupling constant, and $a \sim 246 \text{ GeV}$ is the vacuum expectation value of Higgs. Thus, when properly normalized, the Higgs couplings of the standard model should be proportional to the mass of the particle it couples to. The pattern of deviation from the standard model serves as a powerful probe of the mechanism of mass generation. For example, for a two-Higgs-doublet model where up-type fermion masses are generated by one doublet and down-type fermion masses by another (so-called Type-II two-Higgs-doublet models), the Higgs couplings to all the up-type fermions are shifted by a factor, and those to all the down-type fermions are shifted by another factor. And in models with Radion-Higgs mixing, the Higgs couplings may be reduced uniformly with respect to the standard model values.

4. New Physics Particles

Among the extensions of the standard model, the SUSY models occupy a special place due to their theoretical virtues, the primary one of which is to make the Higgs mass stable in the weak scale. There are also other models that address the same problem, and these models usually contain particles that do not appear in the standard model. One should keep in mind, however, that Nature may have in store for us something that have nothing to do with any of these, and we may be lucky enough to encounter them at LHC/ILC.

4.1 SUSY particles

The MSSM is the most economical model with R -parity conservation which makes the lightest superparticle (LSP) stable. The LSP thus becomes a candidate for the dark matter. The two complex Higgs doublets and the four massless gauge bosons have 8 charged degrees of freedom and 8 neutral degrees of freedom. After breaking of SUSY and gauge symmetries, their super partners mix to form two charginos $\chi_{1,2}^\pm$ (8 degrees of freedom) and four neutralinos $\chi_{1,2,3,4}^0$ (8 degrees of freedom) all with spin 1/2. The neutralinos are self-conjugate; namely, they are Majorana particles. For each fermion f , there are two spin-0 superpartners corresponding to two helicities of the fermion: \tilde{f}_R and \tilde{f}_L which could in general mix, particularly for the third generation fermions. Since the actual masses of each particle and its super-partner are clearly different, the supersymmetry is broken by some mechanism. One popular model is a minimal model with gravity-mediated SUSY breaking (mSUGRA) in which there are only four free parameters and a sign, which may be taken as the mass parameters of scalars and winos: m_0 and M_2 , the trilinear Higgs coupling A_0 , the ratio of vacuum expectation values of the two Higgs doublets, $\tan\beta$, and $\text{sign}(\mu)$ where μ is a Higgs mass parameter. For concreteness, we look for SUSY particles in this section with mSUGRA as a guide.

In many scenarios of SUSY, the super-partners of leptons (sleptons) are light enough to be produced at ILC. In addition, they tend to decay to the corresponding lepton plus the LSP neutralino. In the scenario called SPS1a of mSUGRA, all sleptons decay dominantly as $\tilde{\ell} \rightarrow \ell\chi_1^0$, where ℓ is a lepton and $\tilde{\ell}$ is its super-partner. Decays and interactions of right-handed sleptons are particularly simple since they are $SU(2)_L$ singlets and thus do not interact with $SU(2)_L$ gauge particles. Figure 8 demonstrates simultaneous mass determination of the right-handed smuon $\tilde{\mu}_R$ and the LSP neutralino χ_1^0 in $e^+e^- \rightarrow \tilde{\mu}_R^+\tilde{\mu}_R^-$ followed by $\tilde{\mu}_R^+ \rightarrow \mu^+\chi_1^0$ and its charge conjugate mode. The data is taken well above the threshold with 100 fb^{-1} at 350 GeV CM energy. The smuon and the LSP masses are assumed to be 142 and 118 GeV, respectively. The high and low end points of the

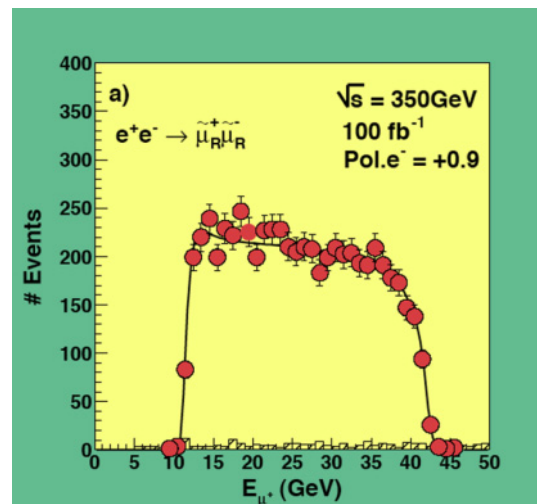


Fig. 8. (Color online) The muon energy distribution in smuon pair production at well above threshold,⁷⁾ $e^+e^- \rightarrow \tilde{\mu}_R^+\tilde{\mu}_R^-$, $\tilde{\mu}_R^+ \rightarrow \mu^+\chi_1^0$. The high and low end points gives both m_χ and $m_{\tilde{\mu}}$.

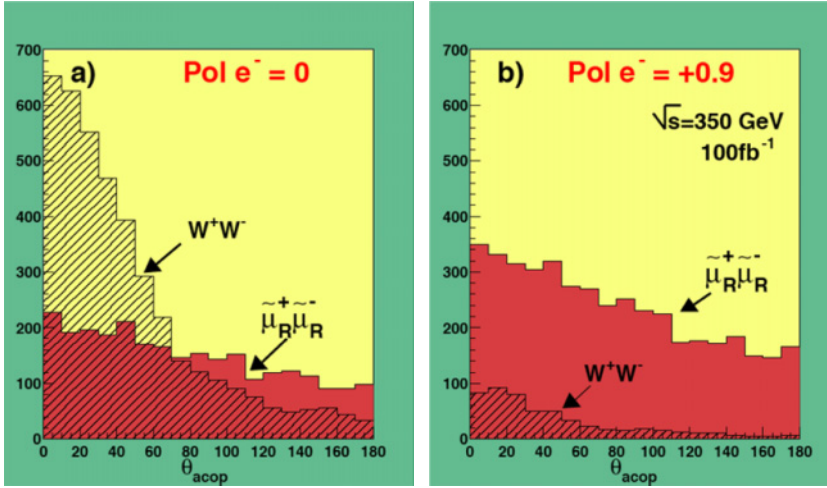


Fig. 9. (Color online) The muon acoplanarity distributions for the smuon production⁷⁾ $e^+e^- \rightarrow \tilde{\mu}_R^+\tilde{\mu}_R^-$, $\tilde{\mu}_R^\pm \rightarrow \mu^\pm\chi_1^0$. With no electron polarization (left) and with 90% electron right-handed polarization.

muon energy distribution gives both masses to a few $\times 10^{-3}$ of themselves. This is in contrast to the LHC case where the mass of LSP is difficult to measure directly. This mode also illustrates the effectiveness of beam polarization in background reduction. The muon acoplanarity distribution in $e^+e^- \rightarrow \tilde{\mu}_R^+\tilde{\mu}_R^-$, $\tilde{\mu}_R^\pm \rightarrow \mu^\pm\chi_1^0$ is shown in Fig. 9 for no electron polarization and with 90% electron polarization. Here, the acoplanarity angle is the angle between the muon pair projected to a plane perpendicular to the beam line. By polarizing the electron right-handedly, one can eliminate the background caused by $e^+e^- \rightarrow W^+W^-$, $W^+ \rightarrow \mu^+\nu$ and its charge conjugate. This is because for the s-channel the initial state e_R^- limits the intermediate state to B (the gauge boson of hypercharge Y) which does not couple to W in the final state, and the t-channel neutrino exchange is a $V-A$ interaction which does not couple to e_R^- .

The angular distribution of the smuon production should be $\sin^2\theta$ since smuon is spin 0 and the intermediate Z/γ state is polarized as $|1, \pm 1\rangle$ along the beam line since the electron coupling to the intermediate state is a linear combination of vector and axial vector. The production angle can be reconstructed with a quadratic ambiguity where the wrong solution has a flat distribution that can be subtracted. The resulting angular distribution can be checked to be consistent with the expected shape.

The smuon mass can also be determined at the threshold, where an energy scan gives the threshold excitation curve which should rise slowly as β_μ^3 due to the P wave nature of the smuon pair.

A large mixing effect is expected for the stau sector and $\tilde{\tau}_R$ and $\tilde{\tau}_L$ would mix to form mass eigenstates $\tilde{\tau}_1$ and $\tilde{\tau}_2$ where $\tilde{\tau}_1$ is defined to be the lighter of the two. The mixing angle can be determined by two or more measurements of $e^+e^- \rightarrow \tilde{\tau}_1^+\tilde{\tau}_1^-$ with different beam polarizations. In the SPS1a scenario mentioned earlier, $\tilde{\tau}_1$ is the lightest of the sleptons with its mass around 100 GeV, and the dominant decay is $\tilde{\tau}_1 \rightarrow \tau\chi_1^0$. In this case, the mixing angle ($\cos 2\theta$) can be determined at the percent level.

The situation for the chargino pair production is similar to that of smuon pair production: $e^+e^- \rightarrow \chi_1^+\chi_1^-$ followed by $\chi_1^\pm \rightarrow \chi_1^0W^\pm$, where the energy distribution of W^\pm simultaneously determines the masses of the chargino χ_1^\pm and the LSP neutralino. With the mass of the LSP obtained in the

smuon study, the mass of the lightest chargino χ_1^\pm can be determined to 1% level.

For neutralinos, the invariant mass distribution of the lepton pair in $e^+e^- \rightarrow \chi_2^0\chi_1^0$ followed by $\chi_2^0 \rightarrow \chi_1^0\ell^+\ell^-$ can determine the mass difference between χ_2^0 and χ_1^0 to better than 1%. This mode may also demonstrate a sizable CP violation effects for some parameter space of MSSM. For example, the sign asymmetry of the T -odd triple product $p_{e^-} \cdot (p_{\ell^+} \times p_{\ell^-})$ can be as large as 20%.²⁷⁾ Similar T -odd triple products can be formed for other modes such as $e^+e^- \rightarrow \chi_1^+\chi_1^-$.

The ability to select the beam polarization allows us to probe into the structures of the SUSY models. For example, the charginos $\chi_{1,2}^\pm$ are the mass eigen states of the system composed of the charged Higgsinos ($\tilde{H}_u^+, \tilde{H}_d^-$) and charged gauginos (\tilde{W}^\pm) where the mass matrix term can be written as

$$\begin{pmatrix} \tilde{W}^+ & \tilde{H}_u^+ \end{pmatrix} \begin{pmatrix} M_2 & \sqrt{2}m_W \cos \beta \\ \sqrt{2}m_W \sin \beta & \mu \end{pmatrix} \begin{pmatrix} \tilde{W}^- \\ \tilde{H}_d^- \end{pmatrix}.$$

By using a right-handed electron beam for $e^+e_R^- \rightarrow \chi_1^+\chi_1^-$, the intermediate s-channel state is purely B which is the gauge boson for hypercharge Y . On the other hand, B couples only to the Higgsino component of chargino; thus, one can obtain information on the mixing parameters of the charginos. Together with cross section measurements of $e^+e_R^- \rightarrow \tilde{e}_R^+\tilde{e}_R^-$ which is sensitive to the mass parameter M_1 which is the mass parameter for Bino (superpartner of B), one can perform a global fit to the parameters ($M_1, M_2, \mu, \tan \beta$). Figure 10 shows the result of the global fit. If the masses M_1 and M_2 are to converge to a single value at the GUT scale, they would satisfy the GUT relation

$$M_1 = \frac{5}{3} \tan^2 \theta_W M_2,$$

which is tested in a highly model independent way.

In most SUSY scenarios, squarks are in general heavier than sleptons and many of them are beyond the reach of ILC even with the energy upgrade to 1 TeV. Still, due to the large mixing effects expected for the third generation squarks \tilde{t} and \tilde{b} , the lighter ones, \tilde{t}_1 and \tilde{b}_1 , can be within reach of ILC. When they can be pair produced as in

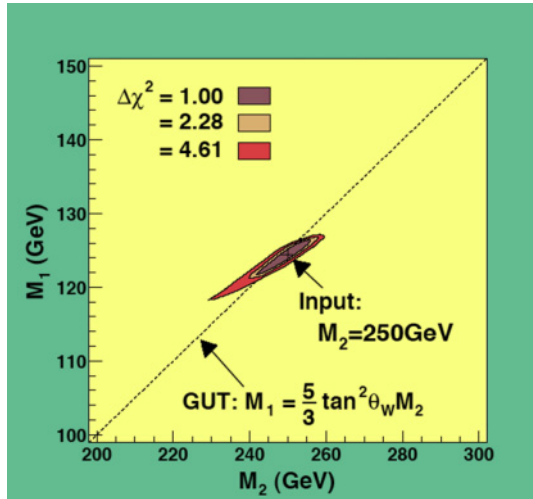


Fig. 10. (Color online) The result of a global fit⁷⁾ to $e^+e^- \rightarrow \tilde{e}_R^+ \tilde{e}_R^-$ and $e^+e^- \rightarrow \chi_1^+ \chi_1^-$. The line shows the GUT relation between M_1 and M_2 .

$e^+e^- \rightarrow \tilde{t}_1 \tilde{t}_1$, then multiple measurements of cross sections with different beam polarizations can determine the mixing angle just as in the case of the stau pair production with a similar precision.

4.2 KK mode gravitons

In the models with large extra dimensions where only gravitons can propagate in the extra dimensions, the fundamental gravity mass scale M_D can be as small as the TeV scale.³⁾ When the wave function of the graviton has a certain number of nodes in the direction of the extra dimensions (KK modes), it can have mass as a function of the number of nodes. When the number of the extra dimension δ is 2 to 6, the size of extra dimension can be very large and is around 0.1 mm to 1 fm, for which the KK mode graviton G_{KK} has effectively a continuous mass spectrum. At ILC, one may search for emission of KK mode graviton in $e^+e^- \rightarrow \gamma G_{KK}$ where G_{KK} escapes the detector and appear as missing energy. Here again, the beam polarization is a powerful handle to suppress the main background $e^+e^- \rightarrow \nu \bar{\nu} \gamma$. With 1 ab^{-1} at 800 GeV and with the electron and positron beam polarizations of 80 and 60% respectively, the 95% confidence level lower limit of M_D is 10 (3) TeV for δ of 2 (6). This is similar to the sensitivities at LHC. At ILC, however, one can utilize the angular distribution of γ to verify the spin of G_{KK} which should be two. In addition, the number of extra dimension δ can be measured at ILC by the energy dependence of the cross section, say at 500 GeV vs at 800 GeV, and the missing mass distribution.

4.3 Little Higgs models

In the Little Higgs models, the Higgs particle is composite, and there exist extra gauge bosons and top partners.⁴⁾ Most new particles are too heavy to be directly detected at ILC, but indirect search for extra gauge bosons is possible with $e^+e^- \rightarrow f \bar{f}$ as described earlier (Fig. 2). Furthermore, in the model with T -parity, there could be a pseudo-axion η below 1 TeV. In such cases, $e^+e^- \rightarrow ZHH$ can be substantially enhanced by $ZH\eta$ coupling: $e^+e^- \rightarrow Z^* \rightarrow \eta^* H, \eta^* \rightarrow ZH$ which should be easily detectable with the TeV upgrade of the machine.

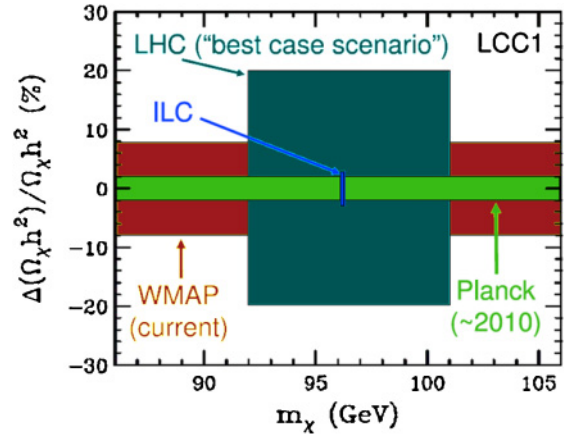


Fig. 11. (Color online) The error in Ω_{DM} vs the lightest neutralino mass as constrained by LHC and ILC data within the framework of mSUGRA with parameter set SPS1a.²⁸⁾

4.4 Cosmological connections

The WMAP satellite data indicates that the cold dark matter density of the universe is given by $\Omega_{DM} h^2 = 0.113 \pm 0.009$ and makes up about 1/4 of the energy of the universe.²⁶⁾ The error on Ω_{DM} will be reduced significantly by the Planck measurements expected around 2010. In the MSSM, the lightest neutralino χ_1^0 serves as a candidate for the cold dark matter. In order to predict the relic density of the cold dark matter, however, all interactions contributing to χ_1^0 annihilation should be known. Figure 11 shows the result of a study within the mSUGRA SPS1a scenario. The sensitivities of LHC and ILC in the two-dimensional space of $m_{\chi_1^0}$ and the estimated error on Ω_{DM} are shown together with the uncertainties on Ω_{DM} by WMAP and Planck. ILC can determine the mass of χ_1^0 much more accurately than LHC, and the error on the estimate of Ω_{DM} is comparable to the error expected for the future measurement by Planck.

5. Options: $\gamma\gamma$ and e^-e^- Colliders

The e^+e^- mode of ILC can accommodate e^-e^- and $\gamma\gamma$ colliders with relatively minor modifications. The $\gamma\gamma$ collider requires a pair of powerful lasers that are aimed at the interaction point from both sides along the beam line. The photons that are Compton back-scattered by incoming beams collide at the interaction point. The maximum CM energy of the $\gamma\gamma$ collision is only slightly lower than that of the e^+e^- collision, and the luminosity is also comparable. The disrupted beams, however, need to be extracted without hitting the sensitive detector parts, and this necessitates a crossing angle greater than 25 mrad (compared to the nominal 14 mrad). Also, the original beams also collide on top of the $\gamma\gamma$ collisions, and this favors the e^-e^- mode over the e^+e^- mode which has larger total cross section. The e^-e^- is suited for the $\gamma\gamma$ collision also because it is easier to produce polarized electrons than polarized positrons.

The Higgs particle can be produced by the s-channel $\gamma\gamma \rightarrow H$ process which involves loop diagrams of charged particles. It allows a precision measurement of the Higgs coupling to photon and is sensitive to new particles that can contribute in the loop. The Higgs mass reach is close to the

CM energy of the e^-e^- beams itself. Higgs below 140 GeV would be detected in the $b\bar{b}$ final state. With 410 fb of $\gamma\gamma$ luminosity at the beam CM energy of 210 GeV, and for $m_H = 120$ GeV, $\Gamma(H \rightarrow \gamma\gamma) \times Br(H \rightarrow b\bar{b})$ can be determined to a statistical error of 2%.²⁹⁾ Even for heavy Higgs of 200 to 350 GeV, the two photon width can be determined with errors of 3 to 10%. The total Higgs decay width can be obtained by combining the $\Gamma(H \rightarrow \gamma\gamma)$ measurement with $Br(H \rightarrow \gamma\gamma)$ measured at the e^+e^- collider at high CM energy. The expected error on the Higgs total width is about 5% for $m_H = 120$ to 140 GeV, which is competitive with the method using $\Gamma_H = \Gamma(H \rightarrow WW^*)/Br(H \rightarrow WW^*)$ mentioned earlier.

The e^-e^- collider can generate exotic charge two particles in s-channel. It is also sensitive to Majorana neutrino exchange in $e^-e^- \rightarrow W^-W^-$. The neutralino exchange interactions $e^-e^- \rightarrow e_{L,R}^-e_{L,R}^-$ allows one to study the quantum numbers of selectrons through beam polarizations.

6. Summary

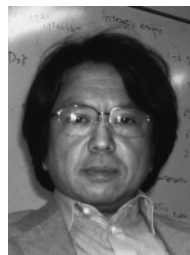
The clean environment and the well-defined initial state of e^+e^- collision, including the spin states, as well as the superb resolutions of the ILC detectors make the ILC physics program very attractive. ILC can study the particles found at LHC in detail to uncover the underlying theoretical structures, and in some cases discover new particles and reactions that are buried in backgrounds at LHC.

Acknowledgment

The author would like to thank the editorial panel of the detector concept report (DCR) who has put together an excellent summary of the ILC physics studies performed so far, and all those who have contributed to these studies. He would like to thank, in particular, Professor Komamiya who has entrusted him to write this article. This work is supported in part by a Grant-in-Aid for Scientific Research 18GS0202 from the Japan Society for the Promotion of Science.

- 1) E. Gildener: *Phys. Rev. D* **14** (1976) 1667, and references therein.
- 2) See, for example, S. Martin: hep-ph/9709356.
- 3) N. Arkani-Hamed, S. Dimopoulos, and G. R. Dvali: *Phys. Rev. D* **59** (1999) 086004, and references therein.

- 4) H.-C. Cheng and I. Low: *J. High Energy Phys.* **JHEP08** (2004) 061, and references therein.
- 5) WWS DCR panel, the detector concept report (DCR) (<http://www.linearcollider.org/wiki/doku.php>).
- 6) Particle Physics at Experiments at JLC, KEK-Report 2001-11.
- 7) "GLC project", KEK Report 2003-7, September 2003.
- 8) "Linear Collider Physics", FERMILAB-Pub-01/058-E, SLAC-R-570, May 2001.
- 9) "TESLA Technical Design Report", DESY-2001-011, March 2001.
- 10) The parameter subcommittee of ILCSC, "The parameters for the linear collider" (<http://www.fnal.gov/directorate/icfa/para-Nov20-final.pdf>).
- 11) LHC/LC study group: *Phys. Rep.* **426** (2006) 47.
- 12) W. Menges: LC-PHSM-2001-022.
- 13) R. Hawkings and K. Mönig: *EPJ direct* **1** (2000) C8.
- 14) S. Riemann: LC-TH-2001-007.
- 15) A. H. Hoang: hep-ph/0307376, and references therein.
- 16) S. Godfrey, P. Kalyniak, and A. Tomkins: hep-ph/0511335.
- 17) P. Batra and T. M. P. Tait: hep-ph/0606068.
- 18) L. Randall and R. Sundrum: *Nucl. Phys. B* **557** (1999) 79.
- 19) The LEP collaborations and the LEP electroweak working group: hep-ex/0612034.
- 20) G. Degraess, S. Heinemeyer, W. Hollik, P. Slavich, and G. Weiglein: *Eur. Phys. J. C* **28** (2003) 133.
- 21) A. Djouadi, J. Kalinowski, and M. Spira: hep-ph/9704448.
- 22) V. D. Barger, K.-M. Cheung, A. Djouadi, B. A. Kniehl, and P. M. Zerwas: *Phys. Rev. D* **49** (1994) 79.
- 23) M. Kramer, J. H. Kuhn, M. L. Strong, and P. M. Zerwas: *Z. Phys. C* **64** (1994) 21.
- 24) C. Castanier, P. Gay, P. Lutz, and J. Orloff: hep-ex/0101028.
- 25) Y. Yasui *et al.*: hep-ph/0211047.
- 26) D. N. Spergel *et al.* (WMAP collaboration): *Astrophys. J. Suppl.* **148** (2003) 175.
- 27) S. Hesselbach: *Acta Phys. Pol. B* **35** (2004) 2739, and references therein.
- 28) J. Feng: *J. Phys. G* **32** (2006) R1.
- 29) P. Niezurawski, A. F. Zarnecki, and M. Krawczyk: hep-ph/0307183; hep-ph/0307175.



Hitoshi Yamamoto was born in Osaka Prefecture, Japan in 1955. He obtained his B. Sc. (1978) from Kyoto University, and Ph. D. (1985) from California Institute of Technology. He was a research associate at Stanford Linear Accelerator Center (1985–1986), a research associate (1986–1989) and a senior research associate (1989–1990) at Enrico Fermi Institute of University of Chicago, an assistant professor (1991–1993) and an associate professor (1993–1998) at Harvard University, and a professor at University of Hawaii (1998–2001). He has been a professor at Tohoku University since 2001. He has worked extensively on physics of electron-positron storage rings including B factories. His studies have also covered CP violation in neutral K meson system.